AGU PUBLICATIONS

JGR

Journal of Geophysical Research: Space Physics

RESEARCH ARTICLE
10.1002/2014JA019884

Key Points:
- Statistical study of dayside FTEs at Mercury
- FTEs at Mercury have core fields of approximately a few hundred nT and durations ~2–3 s
- FTEs transport ~30% of the flux needed to drive Mercury's substorm cycle

Correspondence to:
S. M. Imber,
si88@leicester.ac.uk

Citation:
Imber, S. M., J. A. Slavin, S. A. Boardsen, B. J. Anderson, H. Korth, R. L. McNutt Jr., and S. C. Solomon (2014), MESSENGER observations of large dayside flux transfer events: Do they drive Mercury's substorm cycle?, *J. Geophys. Res. Space Physics*, *119*, 5613–5623, doi:10.1002/2014JA019884.

Received 14 FEB 2014
Accepted 27 MAY 2014
Accepted article online 31 MAY 2014
Published online 25 JUL 2014

MESSENGER observations of large dayside flux transfer events: Do they drive Mercury's substorm cycle?

Suzanne M. Imber[1,2], James A. Slavin[1], Scott A. Boardsen[3,4], Brian J. Anderson[5], Haje Korth[5], Ralph L. McNutt Jr.[5], and Sean C. Solomon[6,7]

[1]Department of Atmospheric, Oceanic and Space Sciences, University of Michigan, Ann Arbor, Michigan, USA, [2]Department of Physics and Astronomy, University of Leicester, Leicester, UK, [3]Heliophysics Science Division, NASA Goddard Space Flight Center, Greenbelt, Maryland, USA, [4]Goddard Planetary Heliophysics Institute, University of Maryland, Baltimore County, Catonsville, Maryland, USA, [5]The Johns Hopkins University Applied Physics Laboratory, Laurel, Maryland, USA, [6]Department of Terrestrial Magnetism, Carnegie Institution of Washington, Washington, District of Columbia, USA, [7]Lamont-Doherty Earth Observatory, Columbia University, Palisades, New York, USA

Abstract The large-scale dynamic behavior of Mercury's highly compressed magnetosphere is predominantly powered by magnetic reconnection, which transfers energy and momentum from the solar wind to the magnetosphere. The contribution of flux transfer events (FTEs) at the dayside magnetopause to the redistribution of magnetic flux in Mercury's magnetosphere is assessed with magnetic field data acquired in orbit about Mercury by the Magnetometer on the MErcury Surface, Space ENvironment, GEochemistry, and Ranging (MESSENGER) spacecraft. FTEs with core fields greater than the planetary field just inside the magnetopause are prevalent at Mercury. Fifty-eight such large-amplitude FTEs were identified during February and May 2012, when MESSENGER sampled the subsolar magnetosheath. The orientation of each FTE was determined by minimum variance analysis, and the magnetic flux content of each was estimated using a force-free flux rope model. The average flux content of the FTEs was 0.06 MWb, and their durations imply a transient increase in the cross-polar cap potential of ~25 kV. For a substorm timescale of 2–3 min, as indicated by magnetotail flux loading and unloading, the FTE repetition rate (10 s) and average flux content (assumed to be 0.03 MWb) imply that FTEs contribute at least ~30% of the flux transport required to drive the Mercury substorm cycle. At Earth, in contrast, FTEs are estimated to contribute less than 2% of the substorm flux transport. This result implies that whereas at Earth, at which steady-state dayside reconnection is prevalent, multiple X-line dayside reconnection and associated FTEs at Mercury are a dominant forcing for magnetospheric dynamics.

1. Introduction

Mercury's proximity to the Sun means that its magnetosphere is strongly driven by the extreme solar wind conditions at 0.3–0.5 AU. Whereas the solar wind speed at Mercury's orbit is similar to that at Earth (~400 km s^{-1}), the solar wind density is an order of magnitude higher and the interplanetary magnetic field (IMF) strength is ~5 times that at Earth [*Baumjohann et al.*, 2006]. Owing to the planet's comparatively weak dipole moment [*Johnson et al.*, 2012], Mercury's magnetosphere is extremely small, on occasion barely holding the solar wind off the planetary surface. A combination of the extreme solar wind conditions and fast transit times through the small magnetosphere cause Mercury's magnetosphere to experience much greater solar wind forcing than Earth's system [*Slavin et al.*, 2009]. The large-scale dynamic behavior of Mercury's highly compressed magnetosphere is predominantly powered by magnetic reconnection, which transfers energy and momentum from the solar wind to the magnetosphere. Low-latitude dayside reconnection, combined with reconnection between the lobes of the magnetotail, drive Mercury's substorm cycle, which circulates magnetic flux through the system [e.g., *Slavin et al.*, 2009; *Sundberg et al.*, 2012].

Reconnection takes place at low latitudes on Earth's magnetopause wherever the angle between the sheath field and the planetary field (known as the shear angle) is high [e.g., *Dungey*, 1961; *Sonnerup*, 1974; *Cowley and Lockwood*, 1992]. This process opens magnetic field lines to the solar wind and increases the open flux content of the magnetosphere, driving the Dungey cycle of magnetic flux circulation. Direct observations of reconnection sites are extremely rare, but observations of reconnection-related phenomena such as magnetic structures known as flux transfer events (FTEs) [e.g., *Russell and Elphic*, 1978; *Berchem*

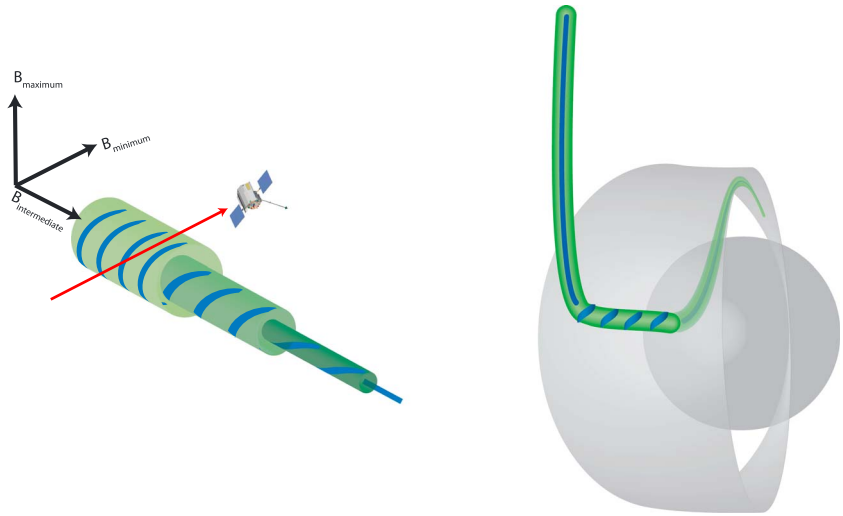

Figure 1. Schematic views of (left) the internal magnetic field structure of a flux rope (magnetic field lines through the structure are shown in blue) and (right) the characteristic location and orientation of a newly formed FTE at Mercury's dayside magnetopause. The planet and the magnetopause are represented by the grey-shaded surfaces with the Sun out of the page and to the left of the schematic view. The newly formed FTE is shown in green, and the blue line follows a magnetic field line through the structure.

and Russell, 1984] and reconnection outflow [e.g., *Phan et al.*, 2000] with embedded magnetic fields normal to the magnetopause indicate ongoing reconnection [*Sonnerup et al.*, 1990].

Flux transfer events are parcels of hot plasma threaded by open field lines and generated by reconnection at the dayside magnetopause. They have been extensively studied at Earth, and they were first detected at Mercury from Mariner 10 data [*Russell and Walker*, 1985]. They have been reported more recently in the MErcury Surface, Space ENvironment, GEochemistry, and Ranging (MESSENGER) observations and are remarkably prevalent [*Slavin et al.*, 2009, 2010a, 2010b, 2012]. There are two formation mechanisms for FTEs, which both involve reconnection but generate structures with subtly different characteristics. The single X-line theory, proposed by *Southwood et al.* [1988] and *Scholer* [1988], attributes a bulge of reconnected flux to a short-duration increase in the reconnection rate at a single X-line. This reconnected flux and the draping signature of the field lines around it form the FTE. The second theory invokes multiple parallel X-lines reconnecting field lines either sequentially or simultaneously [e.g., *Lee and Fu*, 1985; *Raeder*, 2006]. With precisely antiparallel magnetic fields (180° shear angle), two-dimensional closed "O" lines would be formed, but a guide field is almost always present, resulting in the formation of a three-dimensional helical structure. Both mechanisms yield reconnected flux tubes that are magnetically connected to the planetary magnetic field and the solar wind (see Figure 1) and move away from the reconnection site at the local Alfvén speed in the frame of reference of the X-line, but only multiple X-line reconnection produces FTEs with a flux rope topology directly.

The flux rope structure of FTEs was first identified by *Saunders et al.* [1984] and *Rijnbeek et al.* [1984] and has been confirmed by Grad-Shafranov reconstructions of FTEs at Earth [e.g., *Sonnerup et al.*, 2004; *Hasegawa et al.*, 2006]. Flux ropes are magnetic structures containing helical magnetic field lines with a large twist relative to the flux rope axis in the outer regions, so that the structure is more axially aligned toward the center. Observations of the strong magnetic field at the center of the flux rope, termed the core field, can be used to determine whether a spacecraft has entered the flux rope itself or rather observed only the draping of the magnetic field outside the structure. A schematic view of a flux rope shortly after formation is shown in Figure 1.

At Earth, FTEs have been observed at all locations on the magnetopause, from the dayside to the flanks and the postterminator regions, from measurements by the International Sun-Earth Explorer (ISEE) [e.g., *Russell and Elphic*, 1979], Interball [e.g., *Korotova et al.*, 2012], Active Magnetospheric Particle Tracer Explorers (AMPTE) [e.g., *Sanny et al.*, 1998], Cluster [e.g., *Wild et al.*, 2005; *Dunlop et al.*, 2005; *Fear et al.*, 2007], and the Time History of Events and Macroscale Interactions during Substorms (THEMIS) spacecraft [e.g., *Hasegawa*

et al., 2010]. Typical FTE signatures span several minutes, and they have a characteristic repetition time of ~8 min [e.g., *Rijnbeek et al.*, 1984; *Kuo et al.*, 1995; *Sanny et al.*, 1998]. Calculations of their flux content indicate that these features account for only a small fraction (~2%) of the total flux transport needed to drive the substorm cycle at Earth [e.g., *Huang et al.*, 2009]. If the flux ropes are formed at multiple X-lines, the vast majority of the open flux transport is provided by reconnection at single X-lines or steady state reconnection.

Observations of magnetopause crossings at Mercury show that large magnetic field components normal to the magnetopause are observed for nearly all IMF orientations [*DiBraccio et al.*, 2013], implying that reconnection occurs even at very low shear angles, likely because of the low Alfvén Mach number and low values of β, the ratio of thermal pressure to magnetic pressure, for the plasma in the inner solar system [*Slavin and Holzer*, 1979]. This result supports the findings of *Slavin et al.* [2009], who analyzed magnetic field observations during the second MESSENGER flyby of Mercury and reported a subsolar FTE with a core field that exceeded the magnetic field at closest approach. *Slavin et al.* [2009] also noted that the strength of the magnetic field normal to the magnetopause at Mercury was such that the reconnection rate could be up to 10 times stronger than that at Earth. *Slavin et al.* [2010a] presented the first observations of a substorm, or loading-unloading, cycle at Mercury from data acquired during the third MESSENGER flyby of Mercury and suggested that the relative energy release in loading-unloading events at Mercury is large compared with that at Earth. This result has been confirmed from orbital observations reporting repeated substorm dipolarizations with a quasi-period of 10 s [*Sundberg et al.*, 2012]. The results from MESSENGER have demonstrated that there are fundamental differences between Earth and Mercury in the rate and importance of reconnection. Initial observations of a small number of postterminator FTEs at Mercury reported by *Slavin et al.* [2010b] suggest that these events may contain a large quantity of magnetic flux and play a major role in flux circulation.

In this paper we present the first comprehensive study of the location and flux content of FTEs at Mercury's dayside magnetopause from data acquired by MESSENGER's Magnetometer [*Anderson et al.*, 2007] since the spacecraft's insertion into orbit about Mercury. Our analysis suggests that FTEs contribute at least ~30% of the magnetic flux transport needed to drive Mercury's loading-unloading cycle.

2. Observations

MESSENGER was inserted into a highly inclined, eccentric orbit about Mercury on 18 March 2011. For the period considered here, the outbound portion of the orbit cut through the dayside magnetopause at low latitudes for approximately 15 days out of every Mercury year (88 days). In this study we use the solar-wind-aberrated Mercury solar magnetospheric (MSM′) coordinate system. In this system, the origin is centered on Mercury's internal dipole field, which is aligned with the spin axis and offset 0.2 R_M (where R_M is Mercury's radius, or 2440 km) to the north of the planet's geographic equator [*Anderson et al.*, 2011, 2012]. The X' axis is opposite to the direction of the mean solar wind velocity in Mercury's frame, Z' is directed to magnetic north, and Y' completes the right-handed system. The aberration uses an average radial solar wind speed of 400 km s^{-1} and Mercury's orbital velocity, so that aberrated positive X' is opposite to the solar wind flow in Mercury's frame [*Johnson et al.*, 2012]. In this study we consider 90 orbits during 2012 for which the dayside magnetopause crossing takes place within 1 R_M of $Y' = 0$, spanning the time periods 8 to 25 February and 6 to 23 May 2012. This restriction ensures that the magnetopause crossings occurred in the subsolar region and increases the likelihood of observing FTEs soon after their formation, via component reconnection at a tilted X-line passing through the subsolar point [e.g., *Gonzalez and Mozer*, 1974; *Cowley and Owen*, 1989; *Kawano and Russell*, 1997; *Moore et al.*, 2002; *Trattner et al.*, 2007].

An example of a magnetopause crossing on 16 May 2012 is shown in Figure 2, along with model locations of the magnetopause and bow shock from *Winslow et al.* [2013]. The magnetopause model is that of *Shue et al.* [1997] with a subsolar standoff distance of 1.45 R_M from the internal dipole and a flaring parameter of $\alpha = 0.5$. The bow shock is a hyperboloid with a standoff distance of 1.95 R_M and an eccentricity of 1.04. For the orbit shown, MESSENGER passed over the northern cusp and crossed the magnetopause near noon at Y', $Z' = [-0.47, 0.20]$ R_M. The magnetic field data measured by the MESSENGER Magnetometer during the 20 min period show two sharp peaks of more than 250 nT magnetic field magnitude just inside the magnetopause.

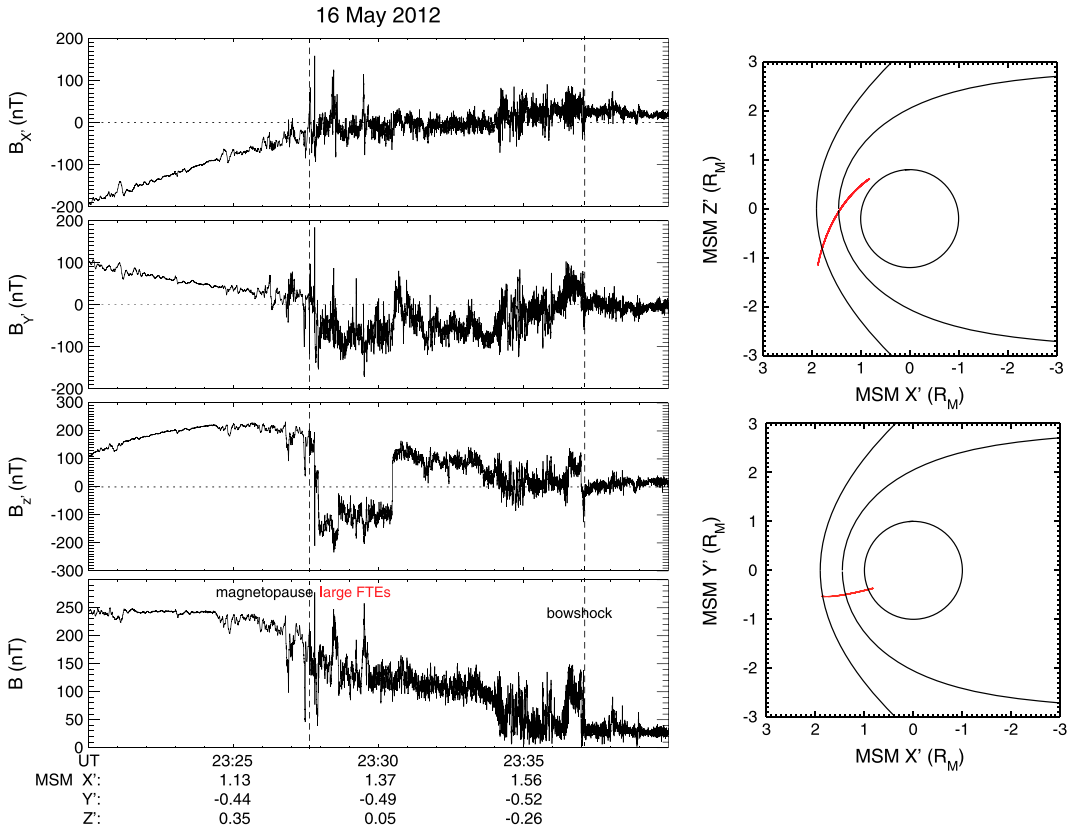

Figure 2. Magnetic field data in MSM′ coordinates during a 40 min interval on 16 May 2012. (left) From top to bottom, the panels show $B_{X'}$, $B_{Y'}$, $B_{Z'}$, and B. Vertical dashed lines mark the approximate locations of the magnetopause and the bow shock according to the models of *Winslow et al.* [2013]. (right) The spacecraft trajectory during this period projected (in red) onto the X'-Z' and X'-Y' planes, along with average model locations for the magnetopause and bow shock (in black).

The magnetic field data from the outbound portion of each of the selected orbits were inspected, and large-amplitude FTEs were identified on the basis of their vector field changes and confirmed with minimum variance analysis (MVA) [*Sonnerup and Cahill*, 1967]. The FTE signature can be observed both inside the magnetopause and in the magnetosheath [*Kuo et al.*, 1995], but in this study we selected only the magnetosheath FTEs as they were substantially easier to identify. These FTEs were initially identified by a short-duration increase in the total magnetic field strength associated with their strong core fields. This criterion allows identification of FTEs of any orientation and direction of motion. A further selection criterion specified that the core field of the FTE was greater than the field strength just inside the magnetopause, ensuring that only large-amplitude FTEs were identified. By restricting analysis to FTE signatures with the strongest fields relative to the magnetospheric field, we also likely restricted consideration to events for which the spacecraft traversed through the core of the FTE.

MVA analysis was then performed on the magnetic field records obtained within each FTE to estimate the orientation of the flux rope axis. Since observations are available from only the single MESSENGER spacecraft, more sophisticated, multi-spacecraft timing analysis to determine the orientation of the FTE axis with greater accuracy is not possible. For a spacecraft passing directly through the center of a flux rope that is nearly force free, the MVA intermediate variance direction is aligned with the long axis of the flux rope, and the minimum and maximum variance directions lie in a plane perpendicular to this axis (see Figure 1). The ratios of the eigenvalues can be used to determine how well this principal axis coordinate system is defined. If the spacecraft did not enter the flux rope but recorded only the draping of the field lines around the structure, or if there were large temporal variations as the spacecraft passed through the FTE, then the axis of minimum variance will not be well defined, and the ratio of the intermediate to minimum variance eigenvectors will be low. Thus, to further ensure that our analysis treated only those cases for which the

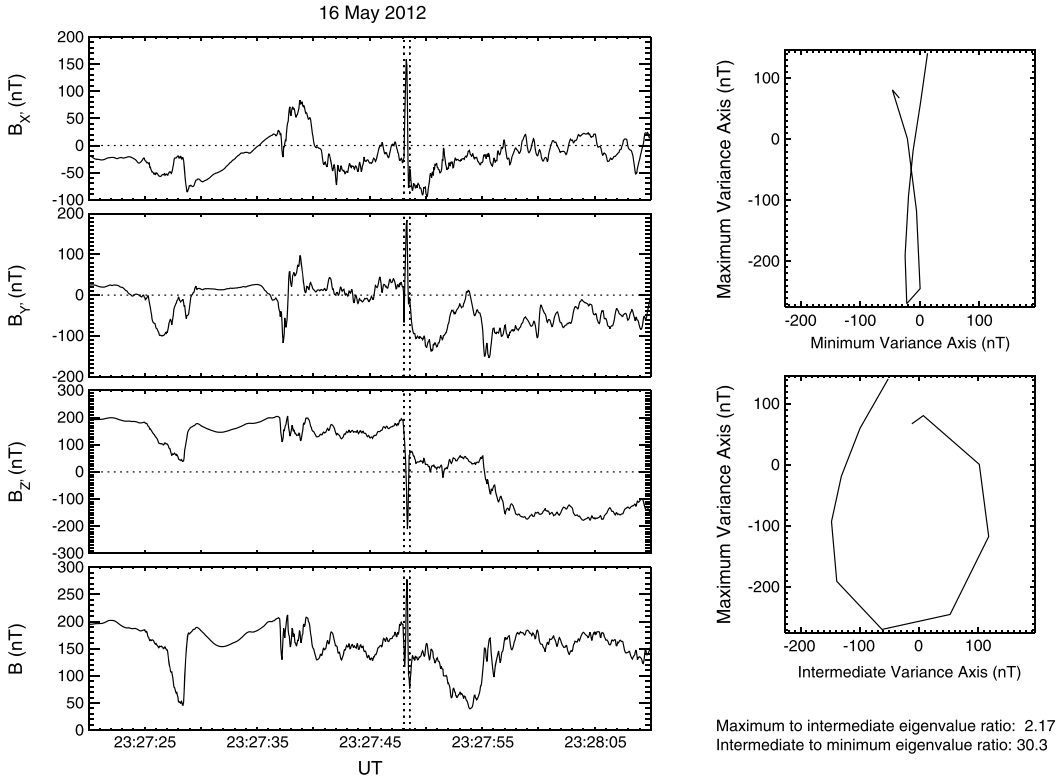

Figure 3. A subset of the data in Figure 2 showing an example of a flux rope. (left) A total of 50 s of magnetic field data are plotted in MSM′ coordinates. The dashed lines mark the start and end times of the FTE; minimum variance analysis was performed on this interval of data. (right) Hodograms of the maximum and minimum variance eigenvalues and maximum and intermediate variance eigenvalues. A clear rotation visible in the latter hodogram represents the rotation of the magnetic field as the flux rope structure was traversed. The ratio of the maximum to intermediate eigenvalue is 2.17, and the ratio of the intermediate to minimum eigenvalue is 30.3.

spacecraft encountered the core of the FTE, we included only those flux ropes for which the ratio of intermediate to minimum variance eigenvalues was greater than 5. In addition, a clear rotation in the hodogram of the maximum and intermediate variance eigenvalues was required to ensure that the FTEs had the structure of a flux rope.

The magnetic field signature of one of the flux ropes identified on 16 May 2012 is shown in Figure 3. The core field of the flux rope reaches 280 nT, a factor of ~1.2 greater than the magnitude of the field just inside the magnetopause. Minimum variance analysis was performed on this interval of data, and the resulting hodograms are shown in Figure 3. The ratio of intermediate to minimum eigenvalue ratio was 30.3, substantially above our threshold of 5, and the hodogram for maximum versus intermediate variance eigenvalues shows a near-360° rotation, as expected for a flux rope. The duration of the FTE in Figure 3 was 0.5 s. Out of a total of 90 orbits, 58 FTEs were identified that fit all of the criteria outlined above. Although the quantitative analysis used here applies only to the large-amplitude FTEs with high ratios of intermediate to minimum variance eigenvalues, it is interesting to note that for every large-amplitude FTE, there were many more FTEs with lower peak magnetic field magnitudes clearly visible in the data. The statistics of these large-amplitude FTEs therefore represents a lower limit on the overall contribution of FTEs to magnetospheric flux transport at Mercury.

3. Modeling and Analysis

3.1. Locations of the FTEs

The location of all 58 FTEs in the MSM *Y′*-*Z′* and *X′*-*Z′* planes are presented in Figures 4a and 4b. Only those orbits for which MESSENGER crossed the magnetopause within ±1 R_M of the noon-midnight meridian have been included, so most of the FTEs lie at low latitudes near the subsolar point. Extreme solar wind

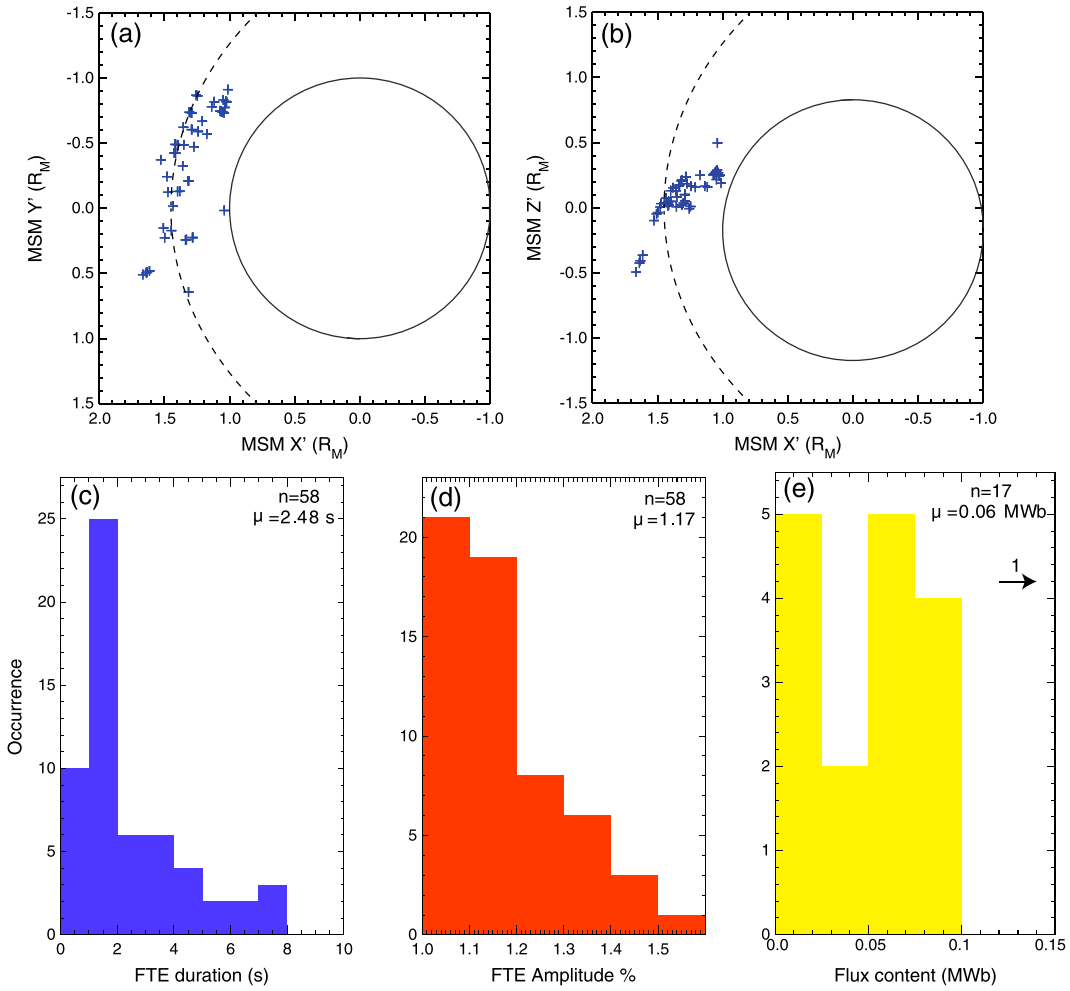

Figure 4. Locations of 58 FTEs identified in this study projected onto (a) the MSM *X'-Y'* and (b) MSM *X'-Z'* planes. The dashed line shows the projections of the average model magnetopause surface shown in Figure 2 from *Winslow et al.* [2013]. Histograms of (c) the duration and (d) the relative amplitude of the 58 FTEs. (e) Magnetic flux content of 17 FTEs derived from a force-free flux rope model. For one of the 17 FTEs, the magnetic flux was 0.22 MWb and off the scale of the figure. The number of FTEs, n, and the mean, μ, of each distribution is indicated.

conditions, of course, may shift the actual location of the magnetopause relative to the average magnetopause shown in the figure. It is interesting to note that more FTEs were observed on the dawn flank, despite approximately even coverage of the dayside magnetopause from dawn to dusk. This outcome could be the result of the IMF sector structure during these intervals favoring reconnection at dawn, or more dawn passes containing multiple FTEs, which will skew the statistics. Further studies with a larger number of events are needed to verify and test explanations for this apparent asymmetry.

There are very few large-scale statistical studies of FTEs at Earth for possible comparison, and the results of these studies are not in agreement. *Wang et al.* [2005] showed an asymmetry between the number of FTEs observed in the dawn and dusk sectors at Earth, but they ruled out the Parker spiral IMF sector as the cause of this asymmetry. Subsequent studies [e.g., *Fear et al.*, 2007; *Korotova et al.*, 2012] indicated that the location of the reconnection site(s) and the subsequent motion of the FTEs are governed primarily by the orientation of the magnetic field in the magnetosheath.

3.2. FTE Amplitudes, Durations, and Flux Content

A histogram of the duration of the FTEs is shown in Figure 4c. The start and end of each FTE signature was determined from changes in the total magnetic field strength, as shown in Figure 2. The mean FTE duration is 2.5 s, and there are very few observed with durations greater than 5 s. In contrast, the average

duration of 100 FTEs identified by *Sanny et al.* [1998] at Earth was 3 min, although the total range was 1 to 9 min. Hence, the FTEs observed at Mercury are ~100 times shorter than those observed at Earth.

FTEs at Earth have typical dimensions of 4000 to over 16,000 km [e.g., *Fear et al.*, 2007]. At Mercury, the subsolar standoff distance is only ~3000 km, so FTEs in Mercury's subsolar region must be smaller than those at Earth. The magnetosheath Alfvén speeds at Mercury are higher than at Earth [*Gershman et al.*, 2013], so FTEs at Mercury are also likely to move at higher speeds. The Fast Imaging Plasma Spectrometer sensor of the Energetic Particle and Plasma Spectrometer on MESSENGER [*Andrews et al.*, 2007] has a minimum integration time of 5 s, so we cannot, in general, directly measure the velocity of these short-duration FTEs with the instrumentation on the MESSENGER spacecraft.

The FTE durations found in this study are somewhat shorter than those previously reported (1–7 s) by *Slavin et al.* [2010b] from data acquired during MESSENGER's first two Mercury flybys. A later study by *Slavin et al.* [2012] investigated FTEs during an "FTE shower" of 66 flux ropes and 97 traveling compression regions observed tailward of the southern cusp. The average duration of FTEs during that shower was 1.7 s. The 2.5 s mean duration of the FTEs studied here is slightly longer than those observed during the shower event, but only the largest-amplitude FTEs were analyzed in this study, a restriction that may have biased the events analyzed to those with longer durations. The FTEs in this paper were observed at low latitudes near noon, suggesting that they are statistically likely to have been observed relatively close to where they were formed, under the assumption of the tilted X-line model discussed earlier.

The maximum magnetic field strength measured during each FTE was divided by the field strength just inside the magnetopause for each pass, to give some indication of the relative amplitude of the FTE core field. These values are underestimates of the core field of the FTEs, since it is unlikely that the center of the flux ropes passed directly over MESSENGER in every case. The distribution of these normalized core field strengths is shown in Figure 4d. Whereas the core field of FTEs at Earth rarely exceeds 50 nT [*Wang et al.*, 2005; *Korotova et al.*, 2012], some of the FTEs in this study have core fields of up to 400 nT, or 160% of the field strength just inside the magnetopause. By comparison, the typical ~1–2 nPa solar wind at 1 AU would produce a magnetic field intensity at Earth's magnetopause of ~50 to 70 nT. For Earth FTEs to match the core fields of the largest FTEs at Mercury, they would need core fields of ~100 nT. This result highlights what we believe to be a fundamental difference between the FTEs at Mercury and those at Earth, namely that FTEs carry a large amount of the available magnetic flux and contribute substantially to the flux transport process as part of the substorm cycle at Mercury.

An estimate of the flux content of these FTEs can be made by modeling them as force-free flux ropes, using a theory first presented by *Lundquist* [1950] and further developed by *Lepping et al.* [1990, 1995, 1996]. The primary assumption is that the gradient in the plasma pressure across the structure is constant, and the outward pressure due to the axial field is precisely matched by the magnetic tension force generated by the large azimuthal field in the outer layers of the flux rope, so the current **J** has no component perpendicular to the magnetic field **B**, or:

$$\nabla \times \mathbf{B} = \mathbf{J} = \alpha \mathbf{B} \tag{1}$$

where α is a proportionality term which determines the amount of twist at the outer edge of the flux rope. It is selected here to be 2.405 so that at the outside of the flux rope the field is purely tangential, and in the center it is purely axial. This approximation has previously been successfully applied to flux ropes in Earth's magnetotail and in the solar wind, although successful fits were achieved only for 50–75% of the flux rope observations [e.g., *Lepping et al.*, 1995; *Slavin et al.*, 2003; *Eastwood et al.*, 2012]. Under the assumption that the variable α is constant, the axial and tangential components of the magnetic field inside the flux rope may be modeled as Bessel functions:

$$\begin{aligned} B_A &= B_0 J_0(\alpha r/R_{fr}) \\ B_T &= H B_0 J_1(\alpha r/R_{fr}) \end{aligned} \tag{2}$$

where B_0 is the magnetic field strength at the core of the flux rope, $J_0(\alpha r/R_{fr})$ and $J_1(\alpha r/R_{fr})$ are the zeroth- and first-order Bessel functions, r is the distance from the center of the flux rope, R_{fr} is the radius of the flux rope, and H is the helicity of the structure.

In this analysis the core field strength, B_0, and the radius of the flux rope, R_{fr}, are not known but must be estimated in the fitting process. To estimate these parameters, we calculate the impact factor, defined as the

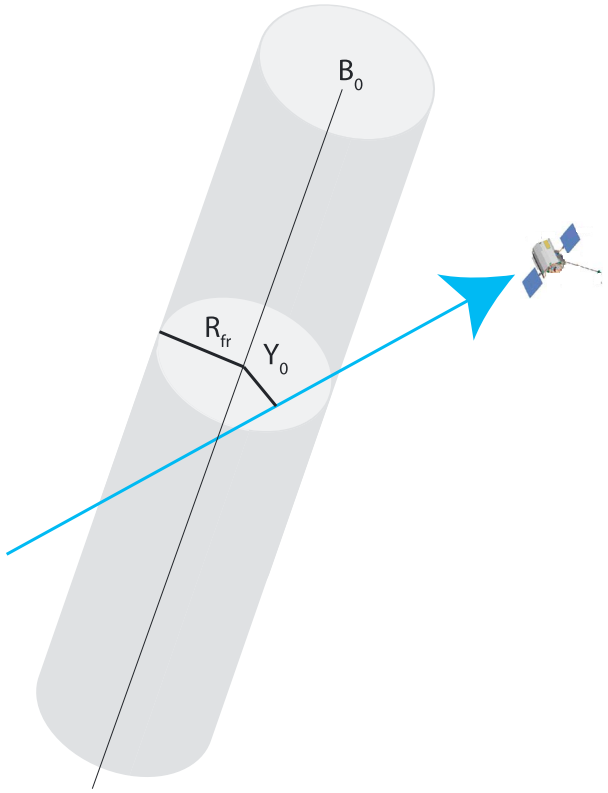

Figure 5. Schematic view of the trajectory of a spacecraft through a model FTE. The spacecraft trajectory is shown in blue, and the flux rope is shown as a grey cylinder. The radius of the flux rope is R_{fr}, the impact factor is Y_0, the core field strength is B_0, and the orientation of the structure is determined from minimum variance analysis.

distance of the spacecraft from the center of the flux rope at the point of closest approach, Y_0. Figure 5 shows the relationship between these parameters. The principal axes of the flux rope are obtained from the minimum variance analysis. We use the ratio of the axial magnetic field strength to the azimuthal field strength at the point of closest approach to obtain the ratio of the impact factor to the flux rope radius, Y_0/R_{fr}. A residual minimization technique then gives the value of the radius that best fits the observed normalized magnetic field data, and this value is scaled to obtain an estimate of the core field strength. In order for this fitting procedure to be judged "successful," a maximum residual level $\chi^2 = 0.04$ was set, a similar criterion to that of *Slavin et al.* [2003] in their study of Geotail observations. More details on this method have been given by *Lepping et al.* [1990, 1995] and *Slavin et al.* [2003].

The equation for calculating the flux content can be shown to be

$$\Phi_{FR} = \left({}^{1}/_{\alpha}\right) 2\pi B_0 R_{fr}^2 J_1(\alpha) \qquad (3)$$

Out of a total of 58 FTEs, 17 have been successfully modeled as force free, and the distribution of their magnetic flux content is shown in Figure 4e. The force-free configuration is thought to be a stable state for a flux rope with constant plasma pressure, but these flux ropes were observed soon after formation and may well contain a substantial fraction of plasma of magnetosheath and magnetospheric origin, so it is not surprising that fits were obtained only for ~30% of the flux ropes.

The main assumption needed to estimate the flux rope radius is the velocity of the flux rope, which moves away from the reconnection site at the local Alfvén speed in the de Hoffman-Teller frame [*Cowley and Owen*, 1989]. Although the magnetosheath density is an order of magnitude higher at Mercury than at Earth, the sheath magnetic field strength is ~5 times higher, so the Alfvén speed in the magnetosheath is likely to be only ~1.5 times higher at Mercury than at Earth. As noted above, the plasma instrument on MESSENGER is unable to measure the FTE velocity directly because the scan time is longer than the duration of an FTE. Calculations of the magnetosheath Alfvén speed at Mercury during time periods surrounding several of the FTEs in this study indicate values of 300–400 km s^{-1} [*Gershman et al.*, 2013]. As the speed of the FTEs cannot be directly measured, we will assume a speed of 400 km s^{-1} in this study, although comparison with average FTE velocities at Earth of ~100–500 km s^{-1} [e.g., *Hasegawa et al.*, 2006; *Fear et al.*, 2007, 2008] suggests that this value may underestimate the actual velocity (and therefore the flux content) of the FTEs at Mercury.

A histogram of the flux content of the FTEs in this study, under the assumption that their speed is 400 km s^{-1}, is presented in Figure 4e. The mean flux content, F, and duration, dt, for these large-amplitude events were 0.06 MWb and 2.5 s, respectively, approximately 10–15% of the flux content of FTEs at Earth [e.g., *Hasegawa et al.*, 2006; *Lui et al.*, 2008; *Zhang et al.*, 2008]. Taking the mean FTE duration at Earth to be 100 s, by Faraday's law, each FTE at Mercury and the Earth contributes dF/dt to the cross-magnetospheric potential, or

0.06 MWb/2.5 s = ~25 kV at Mercury, and 1 MWb/100 s = ~10 kV at Earth. With potential drops of 60 to 120 kV, a transient 10 kV increase at Earth is not a strong electrodynamic perturbation. At Mercury, in contrast, a transient 25 kV increase is large compared with the potential drop of ~20–30 kV estimated by *Slavin et al.* [2009] and *DiBraccio et al.* [2013]. In this study, of course, only the largest FTEs have been analyzed, but even if we assume that the average flux content of FTEs at Mercury is half that estimated for these events, or ~0.03 MWb, each of these FTEs will contribute ~12 kV to the cross polar cap potential. Given the prevalence of FTEs at Mercury [*Slavin et al.*, 2012], it seems likely that FTEs contribute a substantially greater fraction of the total flux transport at Mercury than at Earth.

This conclusion is supported by a comparison of the magnetic flux transport associated with substorms at Earth and Mercury. During the growth, or loading, phase of a substorm, closed magnetic flux on the dayside of the planet is opened and transferred into the tail lobes. The duration of this growth phase at Earth is ~48 min [*Partamies et al.*, 2013], and the ~1.0 MWb FTEs that occur every 8 min are able to contribute ~6 MWb of newly opened magnetic flux during this time. The magnetotail typically contains 12% of the total flux at Earth prior to the onset of the most intense substorms, and on average 0.3 GWb of magnetic flux is cycled [*Milan et al.*, 2007]. The FTEs typically observed at Earth are therefore able to contribute ~2% of the total magnetic flux transfer required to drive a substorm.

The loading phase of substorms at Mercury is thought to last ~90 s, and the tail magnetic flux content is thought to increase by 30–100% [*Slavin et al.*, 2010a]. The average magnetic flux content in the lobes is 2.5 MWb [*Johnson et al.*, 2012], so a conservative estimate of the amount of flux added to the tail during the loading phase is ~1 MWb. If we assume that the average magnetic flux content of FTEs is 0.03 MWb (in this study we found that on average, the largest-amplitude FTEs contain ~0.06 MWb) and that during strong dayside forcing, FTEs occur every 10 s [*Slavin et al.*, 2012], then a conservative estimate of the magnetic flux transferred by FTEs during strong solar wind forcing suggests that 0.3 MWb can be contributed by FTEs alone. This figure is 30% of the total magnetic flux transfer required. With FTEs at Earth transporting only 2% of the total magnetic flux during a substorm growth phase, it is clear that FTEs play a much more substantial role in Mercury's magnetospheric dynamics.

4. Conclusions

A statistical study of 58 FTEs identified in Mercury's magnetosheath near local noon has shown that FTEs at Mercury play a major role in magnetic flux transport. For the 90 orbits during 8–25 February and 6–23 May 2012 selected for this study, the MESSENGER spacecraft crossed the dayside magnetopause within MSM $Y' = \pm 1\ R_M$. Near the dayside magnetopause crossings for these 90 orbits, 58 FTEs with extremely strong core fields were identified from the magnetic field data, and many smaller FTEs were easily visible. Only FTEs with fields larger than the field strength just inside the magnetopause were selected, and the mean ratio of the core field to the magnetopause field was 1.2. The average duration of these large-amplitude FTEs was 2.5 s, substantially shorter than those commonly observed at Earth (for which durations are a few minutes). The core field strengths of the FTEs observed were typically ~250 nT, compared with core fields of a few tens of nT at Earth.

Of the 58 large-amplitude FTEs, 17 were successfully modeled as force-free flux ropes. The average flux content of these large-amplitude FTEs was ~0.06 MWb. For a constant stream of 0.03 MWb FTEs (accounting for the many smaller FTEs visible in the magnetic field data) during a period of intense forcing [e.g., *Slavin et al.*, 2012], the FTEs alone contain at least 30% of the magnetic flux needed to drive a loading-unloading event at Mercury. Although all of the solar wind influences on Mercury's magnetosphere are yet to be identified and understood, it is clear that the system is much more dynamic than Earth's magnetosphere, and FTEs play a major role.

Acknowledgments

S. M. Imber is supported by the MESSENGER project and the European Union Seventh Framework Programme (FP7/2007–2013) under grant agreement 263325. The MESSENGER project is supported by the NASA Discovery Program under contracts NASW-00002 to the Carnegie Institution of Washington and NAS5-97271 to The Johns Hopkins Applied Physics Laboratory. The data used in this study are available from the Planetary Data Center.

Michael Balikhin thanks Tielong Zhang and an anonymous reviewer for their assistance in evaluating this paper.

References

Anderson, B. J., M. H. Acuña, D. A. Lohr, J. Scheifele, A. Raval, H. Korth, and J. A. Slavin (2007), The Magnetometer instrument on MESSENGER, *Space Sci. Rev.*, *131*, 417–450, doi:10.1007/s11214-007-9246-7.

Anderson, B. J., C. L. Johnson, H. Korth, M. E. Purucker, R. M. Winslow, J. A. Slavin, S. C. Solomon, R. L. McNutt Jr., J. M. Raines, and T. H. Zurbuchen (2011), The global magnetic field of Mercury from MESSENGER orbital observations, *Science*, *333*, 1859–1862, doi:10.1126/science.1211001.

Anderson, B. J., C. L. Johnson, H. Korth, R. M. Winslow, J. E. Borovsky, M. E. Purucker, J. A. Slavin, S. C. Solomon, M. T. Zuber, and R. L. McNutt Jr. (2012), Low-degree structure in Mercury's planetary magnetic field, *J. Geophys. Res.*, *117*, E00L12, doi:10.1029/2012JE004159.

Andrews, G. B., et al. (2007), The Energetic Particle and Plasma Spectrometer instrument on the MESSENGER spacecraft, *Space Sci. Rev.*, *131*, 523–556, doi:10.1007/s11214-007-9272-5.

Baumjohann, W., et al. (2006), The magnetosphere of Mercury and its solar wind environment: Open issues and scientific questions, *Adv. Space Res.*, *38*, 604–609.

Berchem, J., and C. T. Russell (1984), Flux transfer events on the magnetopause: Spatial distribution and controlling factors, *J. Geophys. Res.*, *89*, 6689–6703, doi:10.1029/JA089iA08p06689.

Cowley, S. W. H., and M. Lockwood (1992), Excitation and decay of solar wind-driven flows in the magnetosphere-ionosphere system, *Ann. Geophys.*, *10*, 103–115.

Cowley, S. W. H., and C. J. Owen (1989), A simple illustrative model of open flux tube motion over the dayside magnetopause, *Planet. Space Sci.*, *37*, 1461–1475.

DiBraccio, G. A., J. A. Slavin, S. A. Boardsen, B. J. Anderson, H. Korth, T. H. Zurbuchen, J. M. Raines, D. N. Baker, R. L. McNutt Jr., and S. C. Solomon (2013), MESSENGER observations of magnetopause structure and dynamics at Mercury, *J. Geophys. Res. Space Physics*, *118*, 997–1008, doi:10.1002/jgra.50123.

Dungey, J. W. (1961), Interplanetary magnetic field and the auroral zones, *Phys. Rev. Lett.*, *6*, 47–48, doi:10.1103/PhysRevLett.6.47.

Dunlop, M. W., et al. (2005), Coordinated Cluster/Double Star observations of dayside reconnection signatures, *Ann. Geophys.*, *23*, 2867–2875, doi:10.5194/angeo-23-2867-2005.

Eastwood, J. P., T. D. Phan, R. C. Fear, D. G. Sibeck, V. Angelopoulos, M. Øieroset, and M. A. Shay (2012), Survival of flux transfer event (FTE) flux ropes far along the tail magnetopause, *J. Geophys. Res.*, *117*, A08222, doi:10.1029/2012JA017722.

Fear, R. C., S. E. Milan, A. N. Fazakerley, C. J. Owen, T. Asikainen, M. G. G. T. Taylor, E. A. Lucek, H. Rème, I. Dandouras, and P. W. Daly (2007), Motion of flux transfer events: A test of the Cooling model, *Ann. Geophys.*, *25*, 1669–1690, doi:10.5194/angeo-25-1669-2007.

Fear, R. C., S. E. Milan, A. N. Fazakerley, E. A. Lucek, S. W. H. Cowley, and I. Dandouras (2008), The azimuthal extent of three flux transfer events, *Ann. Geophys.*, *26*, 2353–2369.

Gershman, D. J., J. A. Slavin, J. M. Raines, T. H. Zurbuchen, B. J. Anderson, H. Korth, D. N. Baker, and S. C. Solomon (2013), Magnetic flux pileup and plasma depletion in Mercury's subsolar magnetosheath, *J. Geophys. Res. Space Physics*, *118*, 7181–7199, doi:10.1002/2013JA019244.

Gonzalez, W. D., and F. S. Mozer (1974), A quantitative model for the potential resulting from reconnection with an arbitrary interplanetary magnetic field, *J. Geophys. Res.*, *79*, 4186–4194, doi:10.1029/JA079i028p04186.

Hasegawa, H., B. U. Ö. Sonnerup, C. J. Owen, B. Klecker, G. Paschmann, A. Balogh, and H. Rème (2006), The structure of flux transfer events recovered from Cluster data, *Ann. Geophys.*, *24*, 603–618, doi:10.5194/angeo-24-603-2006.

Hasegawa, H., et al. (2010), Evidence for a flux transfer event generated by multiple X-line reconnection at the magnetopause, *Geophys. Res. Lett.*, *37*, L16101, doi:10.1029/2010GL044219.

Huang, C.-S., A. D. DeJong, and X. Cai (2009), Magnetic flux in the magnetotail and polar cap during sawteeth, isolated substorms, and steady magnetospheric convection events, *J. Geophys. Res.*, *114*, A07202, doi:10.1029/2009JA014232.

Johnson, C. L., et al. (2012), MESSENGER observations of Mercury's magnetic field structure, *J. Geophys. Res.*, *117*, E00L14, doi:10.1029/2012JE004217.

Kawano, H., and C. T. Russell (1997), Cause of postterminator flux transfer events, *J. Geophys. Res.*, *102*, 27,029–27,038, doi:10.1029/97JA02139.

Korotova, G. I., D. G. Sibeck, and V. I. Petrov (2012), Interball-1 observations of flux transfer events, *Ann. Geophys.*, *30*, 1451–1462, doi:10.5194/angeo-30-1451-2012.

Kuo, H., C. T. Russell, and G. Le (1995), Statistical studies of flux transfer events, *J. Geophys. Res.*, *100*, 3513–3519, doi:10.1029/94JA02498.

Lee, L. C., and Z. F. Fu (1985), A theory of magnetic flux transfer at the Earth's magnetopause, *Geophys. Res. Lett.*, *12*, 105–108, doi:10.1029/GL012i002p00105.

Lepping, R. P., J. A. Jones, and L. F. Burlaga (1990), Magnetic field structure of interplanetary magnetic clouds at 1 AU, *J. Geophys. Res.*, *95*, 11,957–11,965, doi:10.1029/JA095iA08p11957.

Lepping, R. P., D. H. Fairfield, J. Jones, L. A. Frank, W. R. Paterson, S. Kokubun, and T. Yamamoto (1995), Cross-tail magnetic flux ropes as observed by the Geotail spacecraft, *Geophys. Res. Lett.*, *22*, 1193–1196, doi:10.1029/94GL01114.

Lepping, R. P., J. A. Slavin, M. Hesse, J. A. Jones, and A. Szabo (1996), Analysis of magnetotail flux ropes with strong core fields: ISEE 3 observations, *J. Geomagn. Geoelec.*, *48*, 589–601.

Lui, A. T. Y., D. G. Sibeck, T. Phan, J. P. McFadden, V. Angelopoulos, and K.-H. Glassmeier (2008), Reconstruction of a flux transfer event based on observations from five THEMIS satellites, *J. Geophys. Res.*, *113*, A00C01, doi:10.1029/2008JA013189.

Lundquist, S. (1950), Magneto-hydrostatic fields, *Ark. Fys.*, *2*, 361–365.

Milan, S. E., G. Provan, and B. Hubert (2007), Magnetic flux transport in the Dungey cycle: A survey of dayside and nightside reconnection rates, *J. Geophys. Res.*, *112*, A01209, doi:10.1029/2006JA011642.

Moore, T. E., M.-C. Fok, and M. O. Chandler (2002), The dayside reconnection X line, *J. Geophys. Res.*, *107*(A10), 1332, doi:10.1029/2002JA009381.

Partamies, N., L. Juusola, E. Tanskanen, and K. Kauristie (2013), Statistical properties of substorms during different storm and solar cycle phases, *Ann. Geophys.*, *31*, 349–358, doi:10.5194/angeo-31-349-2013.

Phan, T., et al. (2000), Extended magnetic reconnection at the Earth's magnetopause from detection of bi-directional jets, *Nature*, *404*, 848–850.

Raeder, J. (2006), Flux transfer events: 1. Generation mechanism for strong southward IMF, *Ann. Geophys.*, *24*, 381–392, doi:10.5194/angeo-24-381-2006.

Rijnbeek, R. P., S. W. H. Cowley, D. J. Southwood, and C. T. Russell (1984), A survey of dayside flux transfer events observed by ISEE-1 and ISEE-2 magnetometers, *J. Geophys. Res.*, *89*, 786–800, doi:10.1029/JA089iA02p00786.

Russell, C. T., and R. C. Elphic (1978), Initial ISEE magnetometer results: Magnetopause observations, *Space Sci. Rev.*, *22*, 681–715.

Russell, C. T., and R. C. Elphic (1979), ISEE observations of flux transfer events at the dayside magnetopause, *Geophys. Res. Lett.*, *6*, 33–36, doi:10.1029/GL006i001p00033.

Russell, C. T., and R. J. Walker (1985), Flux transfer events at Mercury, *J. Geophys. Res.*, *90*, 11,067–11,074, doi:10.1029/JA090iA11p11067.

Sanny, J., C. Beck, and D. G. Sibeck (1998), A statistical study of the magnetic signatures of FTEs near the dayside magnetopause, *J. Geophys. Res.*, *103*, 4683–4692, doi:10.1029/97JA03246.

Saunders, M. A., C. T. Russell, and N. Sckopke (1984), Flux transfer events: Scale size and interior structure, *Geophys. Res. Lett.*, *11*, 131–134, doi:10.1029/GL011i002p00131.

Scholer, M. (1988), Magnetic flux transfer at the magnetopause based on single X-line bursty reconnection, *Geophys. Res. Lett.*, *15*, 291–294, doi:10.1029/GL015i004p00291.
Shue, J.-H., J. K. Chao, H. C. Fu, C. T. Russell, P. Song, K. K. Khurana, and H. J. Singer (1997), A new functional form to study the solar wind control of the magnetopause size and shape, *J. Geophys. Res.*, *102*, 9497–9511, doi:10.1029/97JA00196.
Slavin, J. A., and R. E. Holzer (1979), The effect of erosion on the solar wind stand-off distance at Mercury, *J. Geophys. Res.*, *84*, 2076–2082, doi:10.1029/JA084iA05p02076.
Slavin, J. A., R. P. Lepping, J. Gjerloev, D. H. Fairfield, M. Hesse, C. J. Owen, M. B. Moldwin, T. Nagai, A. Ieda, and T. Mukai (2003), Geotail observations of magnetic flux ropes in the plasma sheet, *J. Geophys. Res.*, *108*(A1), 1015, doi:10.1029/2002JA009557.
Slavin, J. A., et al. (2009), MESSENGER observations of magnetic reconnection in Mercury's magnetosphere, *Science*, *324*, 606–610, doi:10.1126/science.1172011.
Slavin, J. A., et al. (2010a), MESSENGER observations of extreme loading and unloading of Mercury's magnetic tail, *Science*, *329*, 665–668.
Slavin, J. A., et al. (2010b), MESSENGER observations of large flux transfer events at Mercury, *Geophys. Res. Lett.*, *37*, L02105, doi:10.1029/2009GL041485.
Slavin, J. A., et al. (2012), MESSENGER observations of a flux-transfer-event shower at Mercury, *J. Geophys. Res.*, *117*, A00M06, doi:10.1029/2012JA017926.
Sonnerup, B. U. (1974), Magnetopause reconnection rate, *J. Geophys. Res.*, *79*, 1546–1549, doi:10.1029/JA079i010p01546.
Sonnerup, B. U., and L. J. Cahill Jr. (1967), Magnetopause structure and attitude from Explorer 12 observations, *J. Geophys. Res.*, *72*, 171–183, doi:10.1029/JZ072i001p00171.
Sonnerup, B. U., I. Papamastorakis, G. Paschmann, and H. Lühr (1990), The magnetopause for large magnetic shear: Analysis of convection electric fields from AMPTE/IRM, *J. Geophys. Res.*, *95*, 10,541–10,557, doi:10.1029/JA095iA07p10541.
Sonnerup, B. U. Ö., H. Hasegawa, and G. Paschmann (2004), Anatomy of a flux transfer event seen by Cluster, *Geophys. Res. Lett.*, *31*, L11803, doi:10.1029/2004GL020134.
Southwood, D. J., C. J. Farrugia, and M. A. Saunders (1988), What are flux transfer events?, *Planet. Space Sci.*, *36*, 503–508.
Sundberg, T., et al. (2012), MESSENGER observations of dipolarization events in Mercury's magnetotail, *J. Geophys. Res.*, *117*, A00M03, doi:10.1029/2012JA017756.
Trattner, K. J., J. S. Mulcock, S. M. Petrinec, and S. A. Fuselier (2007), Location of the reconnection line at the magnetopause during southward IMF conditions, *Geophys. Res. Lett.*, *34*, L03108, doi:10.1029/2006GL028397.
Wang, Y., et al. (2005), Initial results of high-latitude magnetopause and low-latitude flank flux transfer events from 3 years of Cluster observations, *J. Geophys. Res.*, *110*, A11221, doi:10.1029/2005JA011150.
Wild, J. A., et al. (2005), Simultaneous in-situ observations of the signatures of dayside reconnection at the high- and low-latitude magnetopause, *Ann. Geophys.*, *23*, 445–460, doi:10.5194/angeo-23-445-2005.
Winslow, R. M., B. J. Anderson, C. L. Johnson, J. A. Slavin, H. Korth, M. E. Purucker, D. N. Baker, and S. C. Solomon (2013), Mercury's magnetopause and bow shock from MESSENGER Magnetometer observations, *J. Geophys. Res. Space Physics*, *118*, 2213–2227, doi:10.1002/jgra.50237.
Zhang, H., K. K. Khurana, M. G. Kivelson, V. Angelopoulos, Z. Y. Pu, Q.-G. Zong, J. Liu, and X.-Z. Zhou (2008), Modeling a force-free flux transfer event probed by multiple Time History of Events and Macroscale Interactions during Substorms (THEMIS) spacecraft, *J. Geophys. Res.*, *113*, A00C05, doi:10.1029/2008JA013451.